Giant Light Emission Enhancement in Strain-Engineered InSe/MS2 (M = Mo or W) van der Waals Heterostructures

NANO LETTERS

pubs.acs.org/NanoLett
Letter

Giant Light Emission Enhancement in Strain-Engineered InSe/MS_2 (M = Mo or W) van der Waals Heterostructures

Elena Blundo,* Federico Tuzi, Marzia Cuccu, Michele Re Fiorentin, Giorgio Pettinari, Atanu Patra, Salvatore Cianci, Zakhar R. Kudrynskyi, Marco Felici, Takashi Taniguchi, Kenji Watanabe, Amalia Patanè, Maurizia Palummo, and Antonio Polimeni*

Cite This: *Nano Lett.* 2025, 25, 3375−3382
Read Online

ACCESS | Metrics & More | Article Recommendations | Supporting Information

ABSTRACT: Two-dimensional (2D) heterostructures (HSs) offer unlimited possibilities for playing with layer number, order, and twist angle. The realization of high-performance optoelectronic devices, however, requires the achievement of specific band alignments, *k*-space matching between conduction and valence band extrema, and efficient charge transfer between the constituent layers. Fine-tuning mechanisms to design ideal HSs are lacking. Here, we show that layer-selective strain engineering can be exploited as an extra degree of freedom to tailor the band alignment and optical properties of 2D HSs. To that end, strain is selectively applied to MS_2 (M = Mo or W) monolayers in InSe/MS_2 HSs, triggering a giant photoluminescence enhancement of the highly tunable but weakly emitting InSe of up to >2 orders of magnitude. Resonant excitation measurements, supported by first-principles calculations, provide evidence of a strain-activated charge transfer from the MS_2 monolayers toward InSe. The huge emission enhancement of InSe widens its range of applications for optoelectronics.

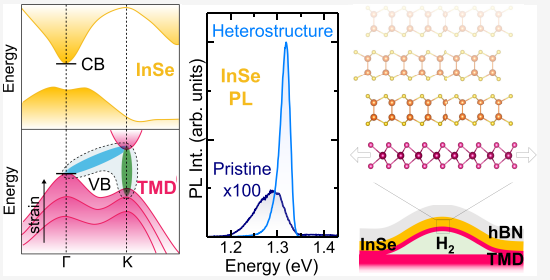

KEYWORDS: *heterostructures, 2D materials, InSe, transition metal dichalcogenides, strain*

van der Waals (vdW) heterostructures (HSs) offer a vast playground for the realization of novel electronic and optoelectronic devices, due to the multitude of degrees of freedom they display, such as layer number, order, and twist angle. The weak vdW adhesion[1] that keeps together different two-dimensional (2D) crystals is responsible for this unprecedented tunability, overcoming lattice mismatch issues and rotational constraints.[2] This high tunability has been exploited to engender novel phenomena, such as superconductivity in twisted multilayer graphene,[3] and to realize efficient electronic devices.[4−9] However, the achievement of high-performance optoelectronic devices remains a challenge due to the necessity to find materials with specific band alignments, *k*-space matching conduction band minima (CBM) and valence band maxima (VBM), and efficient charge transfer between different layers.[10,11] Fine-tuning mechanisms to design ideal HSs are still lacking. Strain has been used to shift the photoluminescence (PL) signal of HSs made of transition metal dichalcogenides (TMDs)[12] and to modify the geometry of the moiré potential in twisted bilayers.[13] In all cases, the entire HS was stretched.

Here, we propose a novel paradigm by selectively straining only one of the constituent materials of vdW HSs formed by MS_2 (M = Mo or W) TMD monolayers (MLs) and InSe thin flakes, resulting in a giant enhancement in the emission efficiency of the latter.

The choice of InSe is grounded in the excellent properties it exhibits. Indeed, InSe features excellent transport properties, such as a high electron mobility[14,15] (1 order of magnitude larger than for MoS_2 and WS_2 MLs[16,17]) and a quasi-direct and tunable optical bandgap (E_{gap}), which makes it particularly appealing, *e.g.*, for fast photodetectors[18] operating from the ultraviolet to the near-infrared range. Indeed, E_{gap} varies from ∼1.2 to ∼2.0 eV, going from bulk to two-layer (L) crystals (for MLs, the lowest-energy transition has an increased indirect character, and it is optically inactive for in-plane polarized light and only weakly coupled to z-polarized light).[15,19]

Research on InSe has rapidly developed, with the fabrication of HSs, such as graphene/InSe,[20] p-InSe/n-In_2O_3,[21] and n-InSe/p-GaSe,[22] resulting in junctions with excellent transport characteristics. InSe/GaSe type II HSs were also exploited to create optically efficient interlayer excitons.[23] The use of InSe for optoelectronic devices, however, is hampered by its relatively low radiative efficiency. As a matter of fact, while the CBM of InSe is located at Γ, the VB has a camel's back shape,

Received: August 30, 2024
Revised: January 9, 2025
Accepted: January 9, 2025
Published: February 5, 2025

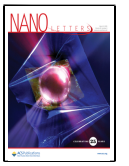

with the VBM slightly off the Γ point (see Figure 1a). For ≳6 layers, the VBM approaches Γ and InSe virtually becomes a direct gap semiconductor.[24] However, the electric dipole orientation of InSe is perpendicular to the exfoliation planes, which leads to a poor coupling to light directed perpendicular to the InSe plane,[24−27] namely, the geometry mainly employed in optical devices. Several works have reported on strategies to increase the optical efficiency of InSe, including bending of the flakes through pillars,[25] ridges,[28] and nanotexturing[29] or the coupling of InSe with inorganic perovskites,[30] but increases of factors of only 2−3 have been typically achieved.

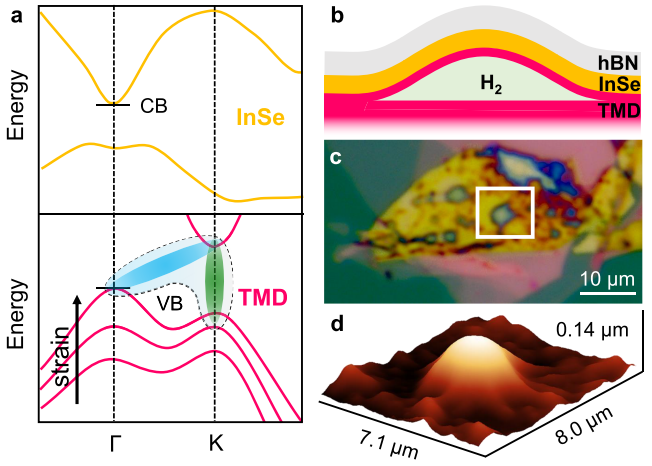

Figure 1. Heterostructured InSe/TMD bubbles. (a) Sketch of the band structure of few-layer-thick InSe and one-layer-thick TMDs. The effect of strain on the VB of TMDs is highlighted. For high strains, the valley at Γ goes above that at K and direct (green) and indirect (cyan) excitons hybridize. (b) Sketch of the system studied in this work, consisting of a heterostructured bubble. A few-layer-thick InSe flake is deposited atop a strained TMD ML in the shape of a bubble; hBN is used to cap the system. (c) Optical image of a flake with heterostructured bubbles. (d) AFM image of the bubble within the white rectangle in panel c.

In a previous work,[31] InSe was coupled to multilayer ($N \geq 2$) TMDs, whose VBM lies at the Γ point. A type II alignment was achieved in such HSs, with the observation of momentum-space direct (at Γ) interlayer excitons, formed by electrons at the InSe CBM and holes at the TMD VBM. Such a system was also exploited for light-emitting transistors.[32] Although these HSs present the advantage of avoiding rotational constraints, their light emission is hindered by poor optical efficiency and significant sample-to-sample fluctuations. These issues can likely be ascribed to the intrinsically low radiative efficiency of InSe (as discussed above) and the *k*-space indirect nature of the bandgap in TMD multilayers. Additionally, these interlayer excitons have comparable intensity to intralayer excitons at cryogenic temperatures, but their spatially indirect nature makes their emission strongly decrease when increasing temperature.[31]

In this work, instead, InSe is coupled to a TMD (MS_2) ML, whose optical bandgap is made indirect (Γ_{VB}−K_{CB}) by strain, yet, at variance with TMD multilayers, it is characterized by a remarkable oscillator strength thanks to the hybridization of direct and indirect exciton states[33,34] (see Figure 1a). In fact, a fine-tuning of strain leads to a unique electronic configuration for the TMD ML in which excitons with an admixed direct−indirect character are observed.[34] In turn, the strained MS_2 ML retains a large light-to-charge conversion. Here, we show that the unique band structure configuration of the HS obtained by this approach, as evaluated by density functional theory (DFT) calculations, enables an efficient strain- and defect-assisted tunneling of photogenerated electrons and holes from the strained ML toward InSe, giving rise to a giant light emission enhancement of InSe.

To create HSs in which only the MS_2 crystal is subject to high strain, while the InSe layer is not, we exploited strained WS_2 and MoS_2 MLs in the shape of microbubbles. The bubbles were created as described in ref 35. Bulk flakes are exposed to a low-energy ionized hydrogen beam; protons penetrate through the topmost layer, and molecular hydrogen forms and accumulates, leading to the formation of microbubbles on the flake surface. Such bubbles mainly have a thickness of just one layer[35,36] and host sizable strains (up to >4%), whose extent increases from the edge toward the center.[1,37,38] Optical spectroscopy and first-principles calcu-

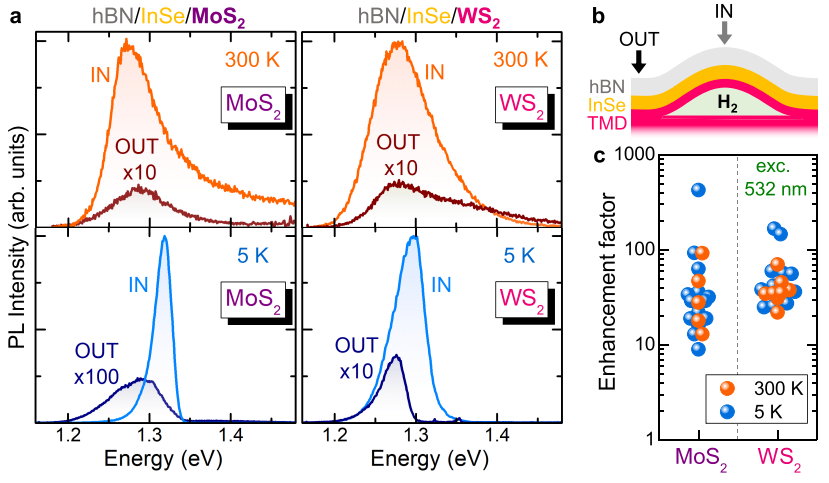

Figure 2. (a) Giant InSe emission enhancement in selectively strained InSe/MS_2 heterostructures. (a) μ-PL spectra at 300 and 5 K of two HS bubbles (one with MoS_2 as the TMD, left, and one with WS_2, right) and of the region right outside the bubble, as indicated in the sketch in panel (b). (c) Summary of the ratios between the PL intensity in the HS bubbles and outside, measured in several MoS_2- and WS_2-based structures at 5 or at 300 K.

https://doi.org/10.1021/acs.nanolett.4c04252
Nano Lett. 2025, 25, 3375−3382

lations revealed that the strain in the bubbles induces a direct-to-indirect transition[33] [with the VBM shifting from K to Γ (see Figure 1a)] and that the nearly resonant direct and indirect excitons hybridize,[34] leading to an efficient PL emission even when the indirect exciton is the lowest-energy state. These properties make strained TMDs promising systems for being coupled with InSe.

InSe and hBN flakes were mechanically exfoliated onto PDMS, and flakes with the desired thickness (∼6−10 L for InSe, <20 nm for hBN) were identified on the basis of their optical contrast. The InSe flakes were then deposited on some selected TMD bubbles; immediately thereafter, hBN was deposited atop the HS to prevent its oxidation[21] (see Methods in the Supporting Information for details). A sketch of the final heterostructured bubble (HS bubble) is shown in Figure 1b, while the optical and three-dimensional atomic force microscope (AFM) images of a real sample are shown in panels c and d, respectively.

The optical properties of the HS bubbles were investigated by excitation with a 532 nm (2.33 eV) laser and by keeping the samples in vacuum to minimize sample oxidation. Micro-PL (μ-PL) measurements were performed from 5 K to room temperature (RT). Interestingly, the heterostructuring process has profound implications on the mechanics of the system in the low-temperature regime. In fact, hydrogen-filled TMD bubbles suddenly deflate at ∼30 K due to the gas-to-liquid phase transition of H_2,[35,39] while we do not observe any major change in the morphology of our HS bubbles even at 5 K (see Note 1 of the Supporting Information). As discussed therein, we attribute this to a tie-beam-like effect played by the InSe/hBN flakes, similar to that characteristic of tied-arch bridges or of Brunelleschi's dome.[40] Raman studies clearly demonstrate that the MS_2 MLs are characterized by biaxial strains of ∼2% and that only a moderate strain reduction is observed with a temperature decrease from RT to 5 K (see Note 2 of the Supporting Information). On the contrary, PL measurements reveal that InSe is subject to minor strains of ∼0.05% (see Note 2 of the Supporting Information).

μ-PL measurements on single HS bubbles, at RT and low temperatures, for both MoS_2 and WS_2, reveal an efficient emission at ∼1.2−1.4 eV (see Figure 2a). This emission corresponds to the intralayer optical emission of InSe (either free or defect-localized[41]), but noticeably, its efficiency is much higher than that typically found in InSe flakes. Given the large spread in intensity (1−2 orders of magnitude) that characterizes InSe flakes with the same thickness,[42] reliable information about the intensity of the HSs can be obtained by a direct comparison within the very same InSe flake. Therefore, in Figure 2, we compare the μ-PL signal recorded on the HS bubble (IN) and right outside (OUT), *i.e.*, where InSe is deposited on the bulk TMD flake and thus not in contact with the TMD ML bubble (see the sketch in panel b). Here, we note that the blue-shift of the IN InSe PL peak with respect to the OUT one apparent at 5 K excludes the possible formation of interlayer excitons and can instead be ascribed to an effective increase in the number of photogenerated carriers in the InSe layer. As we show below, these carriers are injected from the strained TMD ML, eventually leading to a saturation of the InSe lower-energy localized levels and hence to a shift of the PL toward the free exciton states. This scenario is supported by μ-PL studies as a function of T and by low-T power-dependent studies[41,43] on both IN and OUT regions, as discussed in Note 3 of the Supporting Information. The InSe enhancement factor, defined as the ratio between the μ-PL peak intensities detected IN and OUT (I_{IN}/I_{OUT}, where I is the peak intensity), may show some variation with temperature, although an unequivocal trend cannot be found. Nevertheless, an indubitable emission enhancement between 1 and >2 orders of magnitude is systematically observed, as shown by a statistical analysis of several HS bubbles (see Figure 2c). It should be noted that the enhancement factors displayed in the figure were measured under nonresonant conditions, namely by excitation with a 532 nm laser. As shown below, even larger PL intensities can be detected by pumping in resonance with the TMD excitons.

As discussed in Note 4 of the Supporting Information, we created several control samples to verify that there is no enhancement in the absence of strain and that the enhancement is due to strain solely and not to interference or exciton−dipole orientation effects. The giant PL enhancement of InSe in InSe/MS_2 HS bubbles can thus be explained by hypothesizing a strain-induced charge transfer from the MS_2 layer toward InSe. To ascertain this, we performed μ-PL excitation (μ-PLE) measurements on both hBN/InSe/MoS_2 and hBN/InSe/WS_2 HS bubbles (see Figure 3). Noticeably, clear exciton

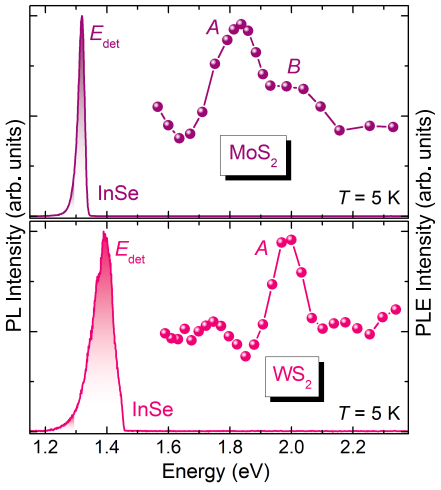

Figure 3. Energy-resonant photoexcited carrier transfer. PLE spectra of (a) a HS bubble based on MoS_2 and (b) a HS bubble based on WS_2. The corresponding PL band whose intensity was detected during the PLE measurements is displayed. Exciton resonances attributable to the A and B excitons of the TMD are highlighted.

resonances are observed. For hBN/InSe/MoS_2 HS bubbles, two resonances are found, at 1.84 and 2.01 eV. The former, attributed to the direct A exciton, is red-shifted by ∼0.1 eV with respect to the A exciton in planar MoS_2 MLs due to strain.[33,44] The second resonance at 2.01 eV is ∼0.17 eV above the lowest-energy one. Such a distance is compatible with the A−B exciton distance,[45] and we thus ascribe the 2.01 eV resonance to the B exciton. In hBN/InSe/WS_2 HS bubbles, instead, only one clear resonance, attributed to the A exciton, is observed at 1.98 eV, i.e., ∼0.1 eV below the A exciton in unstrained WS_2 MLs (similar to the MoS_2 case). μ-PLE measurements were also performed in a hBN/InSe/MoS_2 unstrained HS. As shown in Note 5 of the Supporting Information, no resonances were found in the absence of strain. The μ-PLE measurements clearly point to a charge transfer from the MS_2 ML to the InSe flake, which is activated by the strain selectively applied to the MS_2 ML. As a matter of

https://doi.org/10.1021/acs.nanolett.4c04252
Nano Lett. 2025, 25, 3375−3382

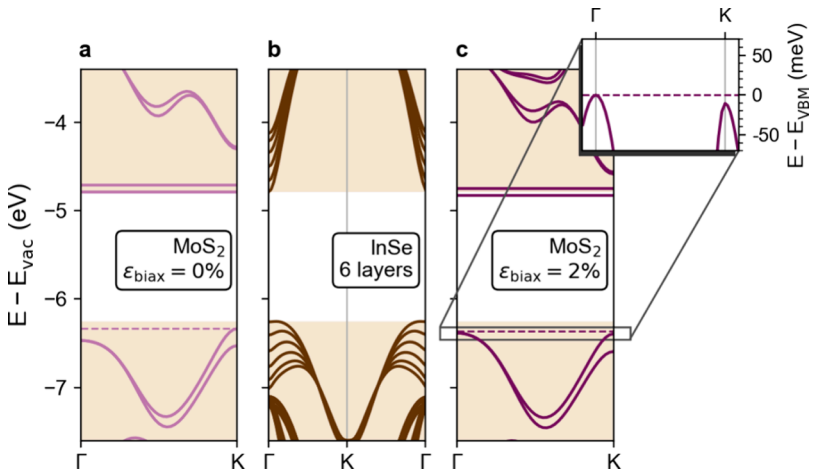

Figure 4. Heterostructured bubble band alignment. DFT-calculated band structures of (a) a MoS_2 ML with S vacancies at 0% strain, (b) a 6L InSe slab, and (c) a MoS_2 ML at 2% biaxial strain. The shaded regions mark the VB and CB of 6L InSe in all panels. The inset of panel c shows a close-up of the top VB of strained MoS_2 at the Γ and K points.

fact, a total strain of ∼0.5% applied to a MoS_2/InSe HS as a whole resulted in no PL enhancement in ref 46. Therefore, our results clearly show that relatively high strains, applied to the MS_2 ML, are required to activate a charge transfer. It should also be noted that such charge transfer is much more efficient than that previously obtained in type I 2D HSs (such as in $MoTe_2$/WSe_2 HSs, where only small PL enhancement factors of ≤2 orders of magnitude could be obtained[47]), which can be attributed to a nearly ideal condition achieved in our case by selective strain engineering.

To further elucidate the effect of strain on such HSs, we performed DFT calculations. The primary factor for ultrafast charge transfer in vdW HSs stems from the band alignment, coupled with the tendency of photoexcited electrons and holes to relax toward the CBM and VBM of the HS, respectively. In the case of type I band alignment, in which both CBM and VBM reside within the same material, like in the present system (see below), upon photoexcitation both electrons and holes migrate across the layers during relaxation. DFT simulations play a pivotal role in understanding charge transfer processes in such systems, providing valuable insights into the fundamental physics and guiding material design and optimization.

Focusing on InSe/MoS_2 HSs, we investigated the electronic band alignment between the MoS_2 ML and a 6L InSe slab. Because defect states, and especially sulfur vacancies, play an important role in determining the electronic properties of TMDs,[48] we also took them into account by including a sulfur vacancy in the MoS_2 ML in the simulation cell. The MoS_2 and InSe bands were aligned to the vacuum level accounting for the interface dipole following the approach of refs 49 and 50. The band structures were computed with the Heyd−Scuseria−Ernzerhof range-separated hybrid functional HSE06[51] (see Methods in the Supporting Information for further details). Panels a and c of Figure 4 show the band structure of the MoS_2 ML at biaxial strains of 0% and 2%, respectively. Such a value was chosen to match the strain estimated through Raman experiments in Note 2 of the Supporting Information. In agreement with previous calculations,[52−57] the application of 2% tensile biaxial strain shifts the VBM from K to Γ (inset of Figure 4c). In the CB, the minimum at the K point rapidly shifts in energy. On the contrary, the S vacancy introduces a pair of flat states within the bandgap, which are minimally affected by strain. It also induces an additional defect state within the VB of MoS_2, in agreement with previous calculations and experiments.[58−60] Lying below the VBM, this level does not impact the proposed charge transfer mechanism and is not shown in Figure 4. The band structure of 6L InSe is displayed in Figure 4b to be readily compared with the MoS_2 unstrained and strained cases.

The computed band structures provide the electronic scenario accounting for the giant PL enhancement of InSe experimentally observed in the HS bubbles. A type I band alignment is found in the absence and presence of strain, and the TMD and InSe VBs feature a sizable overlap around the Γ point (see Figure 4). When they are in contact, charge will equilibrate between the two materials, with the CBM states possibly being partly occupied due to native n-doping, as often experimentally observed.[61,62]

Light is strongly absorbed by the A exciton of MoS_2, mainly due to photoexcited electrons and holes at the K point in the Brillouin zone (BZ). When the TMD ML is unstrained, electrons and holes recombine radiatively at the K point on the picosecond scale[63] and no carrier transfer toward InSe occurs. In contrast, the VBM upshift introduced by tensile strain allows the fast phonon-mediated relaxation of holes from K to Γ, which takes place on the femtosecond scale.[64] In turn, the *k*-space indirect character of the exciton in strained MoS_2 considerably slows its recombination (up to a few nanoseconds[33]). Then, holes in the strained MoS_2 ML can tunnel to InSe at those points in the BZ around Γ, where the bands of the two materials cross and tunneling can efficiently occur without energy or momentum exchange.[65,66] The injected holes radiatively recombine in InSe. Charge is then rebalanced by the relaxation of the photogenerated electron in MoS_2 and the refilling of electrons in the InSe CBM from the TMD ML. Indeed, due to the lack of a fast recombination pathway in the strained TMD ML, electrons in MoS_2 can tunnel to the CBM of InSe, albeit on a time scale longer than that of hole transfer, due to the different *k*-space points of the CB minima in InSe and MoS_2.[46] In this respect, the presence of sulfur vacancies in the TMD ML can contribute to increase the efficiency of the electron transfer to InSe. As shown in Figure 4, the defect levels close to the MoS_2 CBM overlap in energy with the CBM

https://doi.org/10.1021/acs.nanolett.4c04252
Nano Lett. 2025, 25, 3375−3382

of InSe. Electrons populating these states can efficiently tunnel to the InSe CBM, thanks to their *k*-space delocalization that allows for tunneling with relaxed *k*-conservation transfer. Therefore, the density of sulfur vacancies in the TMD monolayer can be an influencing factor in the efficiency of this process, potentially accounting for the variations in the enhancement factor observed in Figure 2b and offering a further degree of control.

Additional defects in InSe, such as Se vacancies, have not been explicitly included in the simulation because they induce localized electronic states below the CBM or above the VBM, which can be readily saturated by the injected carriers.[67−69] The band alignment calculated at the HSE level, in Figure 4, is confirmed by the results obtained from the explicit simulation of the full 6L-InSe/ML-MoS_2 interface, with the Perdew−Burke−Ernzerhof exchange-correlation functional, reported in Note 6 of the Supporting Information. Hence, the concurrent injection of electrons and holes from the strained TMD ML (where efficient light absorption takes place) can populate the band edges of InSe and shift the PL mechanism to more efficient free exciton radiative recombination.

Moreover, we highlight that, for an increasing number of InSe layers, the bandgap slightly decreases (by ∼0.1 eV in going from 6 to 10 layers), so that the results of the calculations performed for 6L InSe can be generalized to *N*L InSe with $6 \leq N \leq 10$ (used in the experiments). A mechanism analogous to that described for InSe/MoS_2 HS bubbles is also expected for WS_2-based HSs. In that case, we remark that while the CBM of WS_2 lies above the CBM of MoS_2 (by ∼0.3 eV[70]), S vacancies in WS_2 monolayers give rise to deeper defect states, emitting ∼0.5 eV below the neutral exciton.[71] In turn, the WS_2 defect band is expected to lie very close in energy to that of MoS_2 and thus be quasi-resonant with the InSe CBM. Finally, we remark that strain in InSe could affect its optical properties[72,73] but would not affect the proposed charge transfer mechanism, as demonstrated by DFT calculations discussed in Note 7 of the Supporting Information.

In this work, we developed a novel paradigm to engineer the optoelectronic properties of 2D HSs by demonstrating how layer-selective stretching can be efficaciously used to tailor the electronic properties of the system. Layer-selective strains can be generally achieved by deposition of 2D flakes on prestretched 2D materials. Here, we specifically investigated the coupling of 6−10-layer-thick InSe with (strained) MS_2 ML bubbles (M = Mo or W). Strain was shown to be responsible for a giant PL enhancement of the InSe signal between 1 and >2 orders of magnitude, at both cryogenic and room temperature. PLE measurements clearly proved that strain activates electronic coupling between the HS constituent layers, entailing a charge transfer from the TMD to InSe. DFT calculations confirm that a type I alignment is obtained and highlight the possible mechanisms responsible for the PL enhancement. This can be attributed to a strain-induced K-to-Γ VBM crossover along with the presence of S vacancy states near the CBM in MS_2, leading to an efficient tunneling of holes (in the vicinity of Γ) and electrons (through momentum-delocalized defect states) at those points in the BZ where electronic states overlap in energy and momentum. In turn, a 2D type I HS characterized by an unprecedentedly efficient charge transfer, much larger than in previous TMD-based HSs, is achieved, thanks to the nearly ideal band alignment triggered by selective strain engineering. The significant enhancement of the PL efficiency of InSe achieved here, paired with its highly remarkable electronic and transport properties, dramatically improves the prospects for the exploitation of this material in a wide range of optoelectronic applications.

■ ASSOCIATED CONTENT

Supporting Information

The Supporting Information is available free of charge at https://pubs.acs.org/doi/10.1021/acs.nanolett.4c04252.

Methods; further morphological, Raman, and PL studies; and further calculations and information about the theoretical model (PDF)

■ AUTHOR INFORMATION

Corresponding Authors

Elena Blundo − *Physics Department, Sapienza University of Rome, 00185 Rome, Italy;* orcid.org/0000-0003-0423-4798; Email: elena.blundo@uniroma1.it

Antonio Polimeni − *Physics Department, Sapienza University of Rome, 00185 Rome, Italy;* orcid.org/0000-0002-2017-4265; Email: antonio.polimeni@uniroma1.it

Authors

Federico Tuzi − *Physics Department, Sapienza University of Rome, 00185 Rome, Italy;* orcid.org/0009-0000-8887-5706

Marzia Cuccu − *Physics Department, Sapienza University of Rome, 00185 Rome, Italy*

Michele Re Fiorentin − *Department of Applied Science and Technology, Politecnico di Torino, 10129 Torino, Italy;* orcid.org/0000-0002-1074-0411

Giorgio Pettinari − *Institute for Photonics and Nanotechnologies, National Research Council, 00133 Rome, Italy;* orcid.org/0000-0003-0187-3770

Atanu Patra − *Physics Department, Sapienza University of Rome, 00185 Rome, Italy*

Salvatore Cianci − *Physics Department, Sapienza University of Rome, 00185 Rome, Italy;* orcid.org/0000-0003-4020-369X

Zakhar R. Kudrynskyi − *Faculty of Engineering, University of Nottingham, Nottingham NG7 2RD, U.K.;* orcid.org/0000-0003-3983-9316

Marco Felici − *Physics Department, Sapienza University of Rome, 00185 Rome, Italy*

Takashi Taniguchi − *Research Center for Materials Nanoarchitectonics, National Institute for Materials Science, Tsukuba 305-0044, Japan;* orcid.org/0000-0002-1467-3105

Kenji Watanabe − *Research Center for Electronic and Optical Materials, National Institute for Materials Science, Tsukuba 305-0044, Japan;* orcid.org/0000-0003-3701-8119

Amalia Patanè − *School of Physics and Astronomy, University of Nottingham, Nottingham NG7 2RD, U.K.;* orcid.org/0000-0003-3015-9496

Maurizia Palummo − *INFN, Dipartimento di Fisica, Università di Roma Tor Vergata, 00133 Rome, Italy*

Complete contact information is available at: https://pubs.acs.org/10.1021/acs.nanolett.4c04252

Author Contributions

E.B. and A. Polimeni conceived and supervised the research. F.T., M.C., and E.B. fabricated the heterostructures. E.B., F.T., M.C., A. Patra, and M.F. performed the optical measurements

https://doi.org/10.1021/acs.nanolett.4c04252
Nano Lett. 2025, 25, 3375−3382

and analyzed the data. M.R.F. and M.P. performed the DFT calculations. G.P. and E.B. performed the AFM measurements and analyzed the data. Z.R.K. and A. Patanè grew the InSe samples. T.T. and K.W. grew the hBN samples. E.B., M.C., M.R.F., M.P., and A. Polimeni wrote the manuscript. The results and the manuscript were approved by all of the co-authors.

Notes

The authors declare no competing financial interest.

■ ACKNOWLEDGMENTS

The authors thank Riccardo Frisenda for discussions. This project was funded within the QuantERA II Programme that has received funding from the European Union's Horizon 2020 research and innovation programme under Grant Agreement 101017733 and with funding organizations Ministero dell'Universitá e della Ricerca (A.Polimeni and M.F.) and Consiglio Nazionale delle Ricerche (G.P.). A.Polimeni and M.F. acknowledge financial support from PNRR MUR Project PE0000023-NQSTI. M.F. and G.P. acknowledge funding from PRIN2022 Project DELIGHT2D (Prot. 20222HNMYE). M.P. acknowledges Union—NextGenerationEU under the Italian National Center 1 on HPC−Spoke 6: "Multiscale Modelling and Engineering Applications". M.R.F. and M.P. acknowledge the Italian Research Center on High Performance Computing, Big Data and Quantum Computing (ICSC), funded by the European Union - NextGenerationEU and established under the National Recovery and Resilience Plan (PNRR), as well as high-performance computing resources provided by CINECA through the ISCRA initiative. Z.R.K. acknowledges funding through a Nottingham Research Fellowship from the University of Nottingham. K.W. and T.T. acknowledge support from the JSPS KAKENHI (Grants 20H00354 and 23H02052) and World Premier International Research Center Initiative (WPI), MEXT, Japan.

■ REFERENCES

(1) Blundo, E.; Yildirim, T.; Pettinari, G.; Polimeni, A. Experimental adhesion energy in van der Waals crystals and heterostructures from atomically thin bubbles. *Phys. Rev. Lett.* **2021**, *127*, 046101.

(2) Geim, A. K.; Grigorieva, I. V. Van der Waals heterostructures. *Nature* **2013**, *499*, 419.

(3) Cao, Y.; Fatemi, V.; Fang, S.; Watanabe, K.; Taniguchi, T.; Kaxiras, E.; Jarillo-Herrero, P. Unconventional superconductivity in magic-angle graphene superlattices. *Nature* **2018**, *556*, 43.

(4) Britnell, L.; Gorbachev, R. V.; Jalil, R.; Belle, B. D.; Schedin, F.; Mishchenko, A.; Georgiou, T.; Katsnelson, M. I.; Eaves, L.; Morozov, S. V.; Peres, N. M.; Leist, J.; Geim, A. K.; Novoselov, K. S.; Ponomarenko, L. A. Field-effect tunneling transistor based on vertical graphene heterostructures. *Science* **2012**, *335*, 947.

(5) Georgiou, T.; Jalil, R.; Belle, B. D.; Britnell, L.; Gorbachev, R. V.; Morozov, S. V.; Kim, Y.-J.; Gholinia, A.; Haigh, S. J.; Makarovsky, O.; Eaves, L.; Ponomarenko, L. A.; Geim, A. K.; Novoselov, K. S.; Mishchenko, A. Vertical field-effect transistor based on graphene−WS_2 heterostructures for flexible and transparent electronics. *Nat. Nanotechnol.* **2013**, *8*, 100.

(6) Britnell, L.; Gorbachev, R. V.; Jalil, R.; Belle, B. D.; Schedin, F.; Katsnelson, M. I.; Eaves, L.; Morozov, S. V.; Mayorov, A. S.; Peres, N. M. R.; Castro Neto, A. H.; Leist, J.; Geim, A. K.; Ponomarenko, L. A.; Novoselov, K. S. Electron tunneling through ultrathin boron nitride crystalline barriers. *Nano Lett.* **2012**, *12*, 1707.

(7) Pospischil, A.; Furchi, M. M.; Mueller, T. Solar-energy conversion and light emission in an atomic monolayer p−n diode. *Nat. Nanotechnol.* **2014**, *9*, 257.

(8) Baugher, B. W.; Churchill, H. O.; Yang, Y.; Jarillo-Herrero, P. Optoelectronic devices based on electrically tunable p−n diodes in a monolayer dichalcogenide. *Nat. Nanotechnol.* **2014**, *9*, 262.

(9) Ross, J. S.; Klement, P.; Jones, A. M.; Ghimire, N. J.; Yan, J.; Mandrus, D. G.; Taniguchi, T.; Watanabe, K.; Kitamura, K.; Yao, W.; Cobden, D. H.; Xu, X. Electrically tunable excitonic light-emitting diodes based on monolayer WSe_2 p−n junctions. *Nat. Nanotechnol.* **2014**, *9*, 268.

(10) Brem, S.; Linderälv, C.; Erhart, P.; Malic, E. Tunable phases of moiré excitons in van der Waals heterostructures. *Nano Lett.* **2020**, *20*, 8534.

(11) Blundo, E.; Tuzi, F.; Cianci, S.; Cuccu, M.; Olkowska-Pucko, K.; Kipczak, Ł.; Contestabile, G.; Miriametro, A.; Felici, M.; Pettinari, G.; Taniguchi, T.; Watanabe, K.; Babiński, A.; Molas, M. R.; Polimeni, A. Localisation-to-delocalisation transition of moiré excitons in WSe_2/$MoSe_2$ heterostructures. *Nat. Commun.* **2024**, *15*, 1057.

(12) Cho, C.; Wong, J.; Taqieddin, A.; Biswas, S.; Aluru, N. R.; Nam, S.; Atwater, H. A. Highly strain-tunable interlayer excitons in MoS_2/WSe_2 heterobilayers. *Nano Lett.* **2021**, *21*, 3956.

(13) Bai, Y.; Zhou, L.; Wang, J.; Wu, W.; McGilly, L. J.; Halbertal, D.; Lo, C. F. B.; Liu, F.; Ardelean, J.; Rivera, P.; Finney, N. R.; Yang, X.-C.; Basov, D. N.; Yao, W.; Xu, X.; Hone, J.; Pasupathy, A. N.; Zhu, X.-Y. Excitons in strain-induced one-dimensional moiré potentials at transition metal dichalcogenide heterojunctions. *Nat. Mater.* **2020**, *19*, 1068.

(14) Feng, W.; Zheng, W.; Cao, W.; Hu, P. Back gated multilayer InSe transistors with enhanced carrier mobilities via the suppression of carrier scattering from a dielectric interface. *Adv. Mater.* **2014**, *26*, 6587.

(15) Bandurin, D. A.; Tyurnina, A. V.; Yu, G. L.; Mishchenko, A.; Zólyomi, V.; Morozov, S. V.; Kumar, R. K.; Gorbachev, R. V.; Kudrynskyi, Z. R.; Pezzini, S.; Kovalyuk, Z. D.; Zeitler, U.; Novoselov, K. S.; Patanè, A.; Eaves, L.; Grigorieva, I. V.; Fal'ko, V. I.; Geim, A. K.; Cao, Y. High electron mobility, quantum hall effect and anomalous optical response in atomically thin InSe. *Nat. Nanotechnol.* **2017**, *12*, 223.

(16) Yoon, Y.; Ganapathi, K.; Salahuddin, S. How good can monolayer MoS_2 transistors be? *Nano Lett.* **2011**, *11*, 3768.

(17) Radisavljevic, B.; Kis, A. Mobility engineering and a metalinsulator transition in monolayer MoS_2. *Nat. Mater.* **2013**, *12*, 815.

(18) Zhao, Q.; Jie, W.; Wang, T.; Castellanos-Gomez, A.; Frisenda, R. InSe Schottky diodes based on van der Waals contacts. *Adv. Funct. Mater.* **2020**, *30*, 2001307.

(19) Mudd, G. W.; Molas, M. R.; Chen, X.; Zólyomi, V.; Nogajewski, K.; Kudrynskyi, Z. R.; Kovalyuk, Z. D.; Yusa, G.; Makarovsky, O.; Eaves, L.; Potemski, M.; Fal'ko, V. I.; Patanè, A. The direct-to-indirect band gap crossover in two-dimensional van der Waals indium selenide crystals. *Sci. Rep.* **2016**, *6*, 39619.

(20) Bhuiyan, M. A.; Kudrynskyi, Z. R.; Mazumder, D.; Greener, J. D. G.; Makarovsky, O.; Mellor, C. J.; Vdovin, E. E.; Piot, B. A.; Lobanova, I. I.; Kovalyuk, Z. D.; Nazarova, M.; Mishchenko, A.; Novoselov, K. S.; Cao, Y.; Eaves, L.; Yusa, G.; Patanè, A. Photoquantum Hall effect and light-induced charge transfer at the interface of graphene/InSe heterostructures. *Adv. Funct. Mater.* **2019**, *29*, 1805491.

(21) Balakrishnan, N.; Kudrynskyi, Z. R.; Smith, E. F.; Fay, M. W.; Makarovsky, O.; Kovalyuk, Z. D.; Eaves, L.; Beton, P. H.; Patanè, A. Engineering p−n junctions and bandgap tuning of InSe nanolayers by controlled oxidation. *2D Materials* **2017**, *4*, 025043.

(22) Yan, F.; Zhao, L.; Patanè, A.; Hu, P.; Wei, X.; Luo, W.; Zhang, D.; Lv, Q.; Feng, Q.; Shen, C.; Chang, K.; Eaves, L.; Wang, K. Fast, multicolor photodetection with graphene-contacted p-GaSe/n-InSe van der Waals heterostructures. *Nanotechnology* **2017**, *28*, 27LT01.

(23) Zheng, W.; Xiang, L.; de Quesada, F. A.; Augustin, M.; Lu, Z.; Wilson, M.; Sood, A.; Wu, F.; Shcherbakov, D.; Memaran, S.; Baumbach, R. E.; McCandless, G. T.; Chan, J. Y.; Liu, S.; Edgar, J. H.; Lau, C. N.; Lui, C. H.; Santos, E. J.; Lindenberg, A.; Smirnov, D.; Balicas, L. Thickness-and twist-angle-dependent interlayer excitons in

https://doi.org/10.1021/acs.nanolett.4c04252
Nano Lett. 2025, 25, 3375−3382

metal monochalcogenide heterostructures. *ACS Nano* **2022**, *16*, 18695.
(24) Wasala, M.; Sirikumara, H. I.; Raj Sapkota, Y.; Hofer, S.; Mazumdar, D.; Jayasekera, T.; Talapatra, S. Recent advances in investigations of the electronic and optoelectronic properties of group III, IV, and V selenide based binary layered compounds. *J. Mater. Chem. C* **2017**, *5*, 11214.
(25) Mazumder, D.; Xie, J.; Kudrynskyi, Z. R.; Wang, X.; Makarovsky, O.; Bhuiyan, M. A.; Kim, H.; Chang, T.-Y.; Huffaker, D. L.; Kovalyuk, Z. D.; Zhang, L.; Patané, A. Enhanced optical emission from 2D InSe bent onto Si-pillars. *Adv. Opt. Mater.* **2020**, *8*, 2000828.
(26) Brotons-Gisbert, M.; Proux, R.; Picard, R.; Andres-Penares, D.; Branny, A.; Molina-Sánchez, A.; Sánchez-Royo, J. F.; Gerardot, B. D. Out-of-plane orientation of luminescent excitons in two-dimensional indium selenide. *Nat. Commun.* **2019**, *10*, 3913.
(27) Li, C.; Zhao, L.; Shang, Q.; Wang, R.; Bai, P.; Zhang, J.; Gao, Y.; Cao, Q.; Wei, Z.; Zhang, Q. Room-temperature near-infrared excitonic lasing from mechanically exfoliated InSe microflake. *ACS Nano* **2022**, *16*, 1477.
(28) Li, Y.; Wang, T.; Wang, H.; Li, Z.; Chen, Y.; West, D.; Sankar, R.; Ulaganathan, R. K.; Chou, F.; Wetzel, C.; Xu, C. Y.; Zhang, S.; Shi, S. F. Enhanced light emission from the ridge of two-dimensional InSe flakes. *Nano Lett.* **2018**, *18*, 5078.
(29) Brotons-Gisbert, M.; Andres-Penares, D.; Suh, J.; Hidalgo, F.; Abargues, R.; Rodríguez-Cantó, P. J.; Segura, A.; Cros, A.; Tobias, G.; Canadell, E.; Ordejón, P.; Wu, J.; Martínez-Pastor, J. P.; Sánchez-Royo, J. F. Nanotexturing to enhance photoluminescent response of atomically thin indium selenide with highly tunable band gap. *Nano Lett.* **2016**, *16*, 3221.
(30) Andres-Penares, D.; Navarro-Arenas, J.; Sánchez-Alarcón, R. I.; Abargues, R.; Martínez-Pastor, J. P.; Sánchez-Royo, J. F. Enhanced optical response of inse nanosheet devices decorated with $CsPbX_3$ (X = I, Br) perovskite nanocrystals. *Appl. Surf. Sci.* **2021**, *536*, 147939.
(31) Ubrig, N.; Ponomarev, E.; Zultak, J.; Domaretskiy, D.; Zólyomi, V.; Terry, D.; Howarth, J.; Gutiérrez-Lezama, I.; Zhukov, A.; Kudrynskyi, Z. R.; Kovalyuk, Z. D.; Patanè, A.; Taniguchi, T.; Watanabe, K.; Gorbachev, R. V.; Fal'ko, V. I.; Morpurgo, A. F. Design of van der Waals interfaces for broad-spectrum optoelectronics. *Nat. Mater.* **2020**, *19*, 299.
(32) Henck, H.; Mauro, D.; Domaretskiy, D.; Philippi, M.; Memaran, S.; Zheng, W.; Lu, Z.; Shcherbakov, D.; Lau, C. N.; Smirnov, D.; Balicas, L.; Watanabe, K.; Taniguchi, T.; Fal'ko, V. I.; Gutiérrez-Lezama, I.; Ubrig, N.; Morpurgo, A. F. Light sources with bias tunable spectrum based on van der Waals interface transistors. *Nat. Commun.* **2022**, *13*, 3917.
(33) Blundo, E.; Felici, M.; Yildirim, T.; Pettinari, G.; Tedeschi, D.; Miriametro, A.; Liu, B.; Ma, W.; Lu, Y.; Polimeni, A. Evidence of the direct-to-indirect band gap transition in strained two-dimensional WS_2 and MoS_2, and WSe_2. *Phys. Rev. Res.* **2020**, *2*, 012024.
(34) Blundo, E.; Junior, P. E. F.; Surrente, A.; Pettinari, G.; Prosnikov, M. A.; Olkowska-Pucko, K.; Zollner, K.; Woźniak, T.; Chaves, A.; Kazimierczuk, T.; Felici, M.; Babiński, A.; Molas, M. R.; Christianen, P. C. M.; Fabian, J.; Polimeni, A. Strain-induced exciton hybridization in WS_2 monolayers unveiled by Zeeman-splitting measurements. *Phys. Rev. Lett.* **2022**, *129*, 067402.
(35) Tedeschi, D.; Blundo, E.; Felici, M.; Pettinari, G.; Liu, B.; Yildrim, T.; Petroni, E.; Zhang, C.; Zhu, Y.; Sennato, S.; Lu, Y.; Polimeni, A. Controlled micro/nanodome formation in proton-irradiated bulk transition-metal dichalcogenides. *Adv. Mater.* **2019**, *31*, 1903795.
(36) Liu, B.; Yildirim, T.; Lü, T.; Blundo, E.; Wang, L.; Jiang, L.; Zou, H.; Zhang, L.; Zhao, H.; Yin, Z.; Tian, F.; Polimeni, A.; Lu, Y. Variant Plateau's law in atomically thin transition metal dichalcogenide dome networks. *Nat. Commun.* **2023**, *14*, 1050.
(37) Cui, X.; Liu, L.; Dong, W.; Zhou, Y.; Zhang, Z. Mechanics of 2D material bubbles. *Nano Res.* **2023**, *16*, 13434.
(38) Blundo, E.; Surrente, A.; Spirito, D.; Pettinari, G.; Yildirim, T.; Chavarin, C. A.; Baldassarre, L.; Felici, M.; Polimeni, A. Vibrational properties in highly strained hexagonal boron nitride bubbles. *Nano Lett.* **2022**, *22*, 1525.
(39) Cianci, S.; Blundo, E.; Tuzi, F.; Pettinari, G.; Olkowska-Pucko, K.; Parmenopoulou, E.; Peeters, D. B.; Miriametro, A.; Taniguchi, T.; Watanabe, K.; Babinski, A.; Molas, M. R.; Felici, M.; Polimeni, A. Spatially controlled single photon emitters in hBN-capped WS_2 domes. *Adv. Opt. Mater.* **2023**, *11*, 2202953.
(40) Sun, J.; Li, J.; Jiang, Y.; Ma, X.; Tan, Z.; Zhufu, G. Key Construction Technology and Monitoring of Long-Span Steel Box Tied Arch Bridge. *Int. J. Steel Struct.* **2023**, *23*, 191.
(41) Venanzi, T.; Arora, H.; Winnerl, S.; Pashkin, A.; Chava, P.; Patanè, A.; Kovalyuk, Z. D.; Kudrynskyi, Z. R.; Watanabe, K.; Taniguchi, T.; Erbe, A.; Helm, M.; Schneider, H. Photoluminescence dynamics in few-layer InSe. *Phys. Rev. Mater.* **2020**, *4*, 044001.
(42) Mudd, G. W.; Svatek, S. A.; Ren, T.; Patanè, A.; Makarovsky, O.; Eaves, L.; Beton, P. H.; Kovalyuk, Z. D.; Lashkarev, G. V.; Kudrynskyi, Z. R.; Dmitriev, A. I. Tuning the bandgap of exfoliated InSe nanosheets by quantum confinement. *Adv. Mater.* **2013**, *25*, 5714.
(43) Polimeni, A.; Capizzi, M.; Geddo, M.; Fischer, M.; Reinhardt, M.; Forchel, A. Effect of temperature on the optical properties of (InGa)(AsN)/GaAs single quantum wells. *Appl. Phys. Lett.* **2000**, *77*, 2870.
(44) Blundo, E.; Cappelluti, E.; Felici, M.; Pettinari, G.; Polimeni, A. Strain-tuning of the electronic, optical, and vibrational properties of two-dimensional crystals. *Appl. Phys. Rev.* **2021**, *8*, 021318.
(45) Frisenda, R.; Niu, Y.; Gant, P.; Molina-Mendoza, A. J.; Schmidt, R.; Bratschitsch, R.; Liu, J.; Fu, L.; Dumcenco, D.; Kis, A.; De Lara, D. P.; Castellanos-Gomez, A. Micro-reflectance and transmittance spectroscopy: a versatile and powerful tool to characterize 2D materials. *J. Phys. D: Appl. Phys.* **2017**, *50*, 074002.
(46) Sun, Z.-Y.; Li, Y.; Xu, B.; Chen, H.; Wang, P.; Zhao, S.-X.; Yang, L.; Gao, B.; Dou, X.-M.; Sun, B.-Q.; Zhen, L.; Xu, C.-Y. Tailoring the energy funneling across the interface in $InSe/MoS_2$ heterostructures by electrostatic gating and strain engineering. *Adv. Opt. Mater.* **2021**, *9*, 2100438.
(47) Yamaoka, T.; Lim, H. E.; Koirala, S.; Wang, X.; Shinokita, K.; Maruyama, M.; Okada, S.; Miyauchi, Y.; Matsuda, K. Efficient photocarrier transfer and effective photoluminescence enhancement in type I monolayer $MoTe_2/WSe_2$ heterostructure. *Adv. Funct. Mater.* **2018**, *28*, 1801021.
(48) Hong, J.; Hu, Z.; Probert, M.; Li, K.; Lv, D.; Yang, X.; Gu, L.; Mao, N.; Feng, Q.; Xie, L.; Zhang, J.; Wu, D.; Zhang, Z.; Jin, C.; Ji, W.; Zhang, X.; Yuan, J.; Zhang, Z. Exploring atomic defects in molybdenum disulphide monolayers. *Nat. Commun.* **2015**, *6*, 6293.
(49) Hinuma, Y.; Oba, F.; Kumagai, Y.; Tanaka, I. Band offsets of $CuInSe_2$/CdS and $CuInSe_2$/ZnS (110) interfaces: A hybrid density functional theory study. *Phys. Rev. B* **2013**, *88*, 035305.
(50) Hinuma, Y.; Grüneis, A.; Kresse, G.; Oba, F. Band alignment of semiconductors from density-functional theory and many-body perturbation theory. *Phys. Rev. B* **2014**, *90*, 155405.
(51) Heyd, J.; Scuseria, G. E.; Ernzerhof, M. Hybrid functionals based on a screened Coulomb potential. *J. Chem. Phys.* **2003**, *118*, 8207.
(52) Molina-Sánchez, A.; Hummer, K.; Wirtz, L. Vibrational and optical properties of MoS_2: From monolayer to bulk. *Surf. Sci. Rep.* **2015**, *70*, 554.
(53) Zollner, K.; Junior, P. E. F.; Fabian, J. Strain-tunable orbital, spin-orbit, and optical properties of monolayer transition-metal dichalcogenides. *Phys. Rev. B* **2019**, *100*, 195126.
(54) Johari, P.; Shenoy, V. B. Tuning the electronic properties of semiconducting transition metal dichalcogenides by applying mechanical strains. *ACS Nano* **2012**, *6*, 5449.
(55) Chang, C.-H.; Fan, X.; Lin, S.-H.; Kuo, J.-L. Orbital analysis of electronic structure and phonon dispersion in MoS_2, $MoSe_2$, WS_2, and WSe_2 monolayers under strain. *Phys. Rev. B* **2013**, *88*, 195420.
(56) Shi, H.; Pan, H.; Zhang, Y.-W.; Yakobson, B. I. Quasiparticle band structures and optical properties of strained monolayer MoS_2 and WS_2. *Phys. Rev. B* **2013**, *87*, 155304.

https://doi.org/10.1021/acs.nanolett.4c04252
Nano Lett. 2025, 25, 3375−3382

(57) Ghorbani-Asl, M.; Borini, S.; Kuc, A.; Heine, T. Strain-dependent modulation of conductivity in single-layer transition-metal dichalcogenides. *Phys. Rev. B* **2013**, *87*, 235434.
(58) Mitterreiter, E.; Schuler, B.; Micevic, A.; Hernangómez-Pérez, D.; Barthelmi, K.; Cochrane, K. A.; Kiemle, J.; Sigger, F.; Klein, J.; Wong, E.; Barnard, E. S.; Watanabe, K.; Taniguchi, T.; Lorke, M.; Jahnke, F.; Finley, J. J.; Schwartzberg, A. M.; Qiu, D. Y.; Refaely-Abramson, S.; Holleitner, A. W.; Weber-Bargioni, A.; Kastl, C. The role of chalcogen vacancies for atomic defect emission in MoS_2. *Nat. Commun.* **2021**, *12*, 3822.
(59) Zhao, Y.; Tripathi, M.; Čerņevičs, K.; Avsar, A.; Ji, H. G.; Gonzalez Marin, J. F.; Cheon, C.-Y.; Wang, Z.; Yazyev, O. V.; Kis, A. Electrical spectroscopy of defect states and their hybridization in monolayer MoS_2. *Nat. Commun.* **2023**, *14*, 44.
(60) Hötger, A.; Amit, T.; Klein, J.; Barthelmi, K.; Pelini, T.; Delhomme, A.; Rey, S.; Potemski, M.; Faugeras, C.; Cohen, G.; Hernangómez-Pérez, D.; Taniguchi, T.; Watanabe, K.; Kastl, C.; Finley, J. J.; Refaely-Abramson, S.; Holleitner, A. W.; Stier, A. V. Spin-defect characteristics of single sulfur vacancies in monolayer MoS_2. *npj 2D Mater. Appl.* **2023**, *7*, 30.
(61) Ferrer-Roca, C.; Segura, A.; Andrés, M. V.; Pellicer, J.; Muñoz, V. Investigation of nitrogen-related acceptor centers in indium selenide by means of photoluminescence: Determination of the hole effective mass. *Phys. Rev. B* **1997**, *55*, 6981.
(62) Siao, M. D.; Shen, W. C.; Chen, R. S.; Chang, Z. W.; Shih, M. C.; Chiu, Y. P.; Cheng, C. M. Two-dimensional electronic transport and surface electron accumulation in mos2. *Nat. Commun.* **2018**, *9*, 1442.
(63) Moody, G.; Schaibley, J.; Xu, X. Exciton dynamics in monolayer transition metal dichalcogenides. *J. Opt. Soc. Am. B* **2016**, *33*, C39.
(64) Kozawa, D.; Kumar, R.; Carvalho, A.; Kumar Amara, K.; Zhao, W.; Wang, S.; Toh, M.; Ribeiro, R. M.; Castro Neto, A. H.; Matsuda, K.; Eda, G. Photocarrier relaxation pathway in two-dimensional semiconducting transition metal dichalcogenides. *Nat. Commun.* **2014**, *5*, 4543.
(65) Krause, R.; Aeschlimann, S.; Chávez-Cervantes, M.; Perea-Causin, R.; Brem, S.; Malic, E.; Forti, S.; Fabbri, F.; Coletti, C.; Gierz, I. Microscopic understanding of ultrafast charge transfer in van der waals heterostructures. *Phys. Rev. Lett.* **2021**, *127*, 276401.
(66) Hofmann, N.; Weigl, L.; Gradl, J.; Mishra, N.; Orlandini, G.; Forti, S.; Coletti, C.; Latini, S.; Xian, L.; Rubio, A.; Paredes, D. P.; Causin, R. P.; Brem, S.; Malic, E.; Gierz, I. Link between interlayer hybridization and ultrafast charge transfer in WS_2-graphene heterostructures. *2D Mater.* **2023**, *10*, 035025.
(67) Mudd, G. W.; Patanè, A.; Kudrynskyi, Z. R.; Fay, M. W.; Makarovsky, O.; Eaves, L.; Kovalyuk, Z. D.; Zólyomi, V.; Falko, V. Quantum confined acceptors and donors in InSe nanosheets. *Appl. Phys. Lett.* **2014**, *105*, 221909.
(68) Xiao, K. J.; Carvalho, A.; Castro Neto, A. H. Defects and oxidation resilience in inse. *Phys. Rev. B* **2017**, *96*, 054112.
(69) Salomone, M.; Re Fiorentin, M.; Cicero, G.; Risplendi, F. Point defects in two-dimensional indium selenide as tunable single-photon sources. *J. Phys. Chem. Lett.* **2021**, *12*, 10947.
(70) Shree, S.; Paradisanos, I.; Marie, X.; Robert, C.; Urbaszek, B. Guide to optical spectroscopy of layered semiconductors. *Nat. Rev. Phys.* **2021**, *3*, 39.
(71) Micevic, A.; Pettinger, N.; Hötger, A.; Sigl, L.; Florian, M.; Taniguchi, T.; Watanabe, K.; Müller, K.; Finley, J. J.; Kastl, C.; Holleitner, A. W. On-demand generation of optically active defects in monolayer WS_2 by a focused helium ion beam. *Appl. Phys. Lett.* **2022**, *121*, 183101.
(72) Li, Z.-Y.; Cheng, H.-Y.; Kung, S.-H.; Yao, H.-C.; Inbaraj, C. R. P.; Sankar, R.; Ou, M.-N.; Chen, Y.-F.; Lee, C.-C.; Lin, K.-H. Uniaxial strain dependence on angle-resolved optical second harmonic generation from a few layers of indium selenide. *Nanomaterials* **2023**, *13*, 750.
(73) Li, Y.; Niu, X.; Wang, J. Strain-dependent electronic structure and optical properties of monolayer indium selenide: A density functional+tight-binding model+many-body perturbation theory study. *FlatChem.* **2019**, *15*, 100092.

https://doi.org/10.1021/acs.nanolett.4c04252
Nano Lett. 2025, 25, 3375−3382